Supplementary Methods

Movie DR1

Rheology

In order to reproduce and localize deformation in frictional-plastic shear zones, the model uses a plastic yield criterion. Once yielding occurs, materials of the deformed area experience strain softening. In this model, the Drucker-Prager pressure-dependent yield criterion is used to model the plastic behavior for incompressible deformation in plane strain. Yielding occurs when:

$$(J_2)^{\frac{1}{n}} - p\sin\phi(\varepsilon) + c\cos\phi(\varepsilon). \qquad (1)$$

Where $J_2 = \frac{1}{2}\sigma_{ij}\sigma_{ij}$ is the second invariant of the deviatoric stress, p is the dynamic pressure (mean stress), c is the cohesion and ϕ is the internal friction angle. The values of c and $\phi(\varepsilon)$ were chosen to reproduce frictional sliding of rocks. Several mechanisms can lead to brittle weakening of rocks (Huismans and Beaumont, 2007 and references therein), including cohesion loss, mineral transformations, and increased pore fluid pressures. In the models presented here strain weakening is introduced using a parametric approach. The friction angle $\phi(\varepsilon)$ decreases linearly with increasing strain in the range $0.5 < \varepsilon < 1.0$, where ε represents the square root of the second invariant of deviatoric strain.

Model Set Up

The initial model has a computational Eulerian domain 400 km long, 12.5 km high on the left-hand side and 7.5 km high on the right-hand side. The Lagrangian material-tracking grid follows the initial Eulerian domain but extends until 800 km (e.g. Supplementary Table DR1). Materials II and III (representing the sediments and the internal décollement respectively) extend from 100 km to the right-hand side of the model, in order to allow for a first stage of deformation in the internal wedge to occur close to the backstop. Material II is 3 km thick, and Material III is 0.5 km thick, so that Materials II and III have the same thickness on the right-hand side of the model, and the décollement level is located in the middle of the model area. A second décollement level has been added to the base of the model, which is 1 km thick. A velocity of -1 cm.yr^{-1} is applied to the right-hand boundary, while the left-hand side is fixed horizontally, except in the first km, to evacuate the basal décollement layer with a velocity of 1 cm.yr $^{-1}$. The surface is subjected to sedimentation after 5 m.y, represented by the deposition of material with the same properties as Material II below a fixed reference elevation; erosion has not been included in our models. The base of the model is supported by an elastic beam that allows for flexural isostasy.

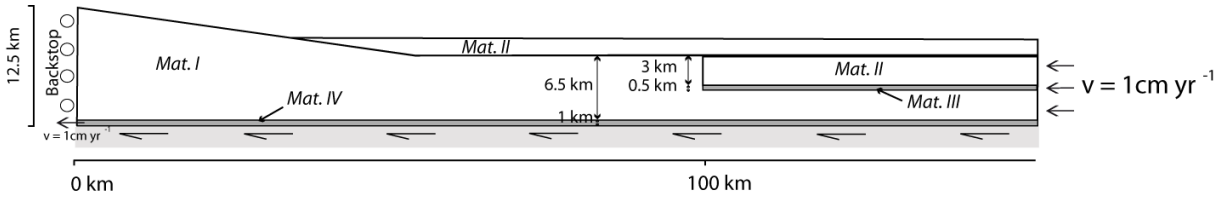

Supplementary Figure DR1: *Initial model geometry.*

Models Parameter Values

Supplementary Table DR1*: Fixed parameter values for numerical model runs.*

Material number	Description		Internal friction angle Φ	
			Φ1	**Φ2**
I	Strong Coulomb, with strain softening		38	25
II	Intermediate Coulomb, with strain softening		38	18
III	Very weak internal décollement		1	
IV	Weak basal décollement		10	
Cohesion	2 MPa			
Density	2300 km.m^{-3}			
Eulerian grid	801 x 81 cells	400 x 12.5 km		
Lagrangian grid	1601 x 81 cells	800 x 12.5 km		

Supplementary Models

Influence of the strength of internal décollement on the thrust sheet lengths

The rheology of the internal décollement can form a major control on the wedge development. In order to test this influence, we have run several models with increasing the strength of the internal décollement material (characterized by its internal friction angle ϕ). We present in supplementary Figure S2 snapshots of models with ϕ at 2°, 4°, 6°, and 8° at the time when the first external thrust activates. Syn-tectonic sedimentation in these supplementary models starts at 3 m.y. and was set at the same level as in the model 2 (Figure 2) for models in panels a to d, and at a higher reference level, covering entirely the basin for models in panels e to h.

Models a-d demonstrate that despite differences in structural styles (in particular in models c and d), the sedimentary thrust sheets formed have a shorter length with increasing décollement strength, ϕ. The first thrust activates at 95, 97, 92 and 84 km from the backstop, in model a, b, c, and d respectively. Models e-h show a similar response to increasing the décollement strength with the higher reference level for sedimentation. The thrusts are shorter for a stronger décollement level, and activate at 112, 107, 86 and 88 km in models e, f, g and h respectively. We note that in models g and h (ϕ = 6° and 8°), the basement and

the sedimentary layers deform jointly, because the difference in strength between the basement, the décollement and the sedimentary layer is small.

We thus conclude from this set of models that the rheology of the décollement level has an impact on the thrust sheet length by shortening them, but this effect is much less significant than the effect of syn-tectonic wedge-top sedimentation on the wedge propagation and thrust sheet length. Moreover, the models confirm that also with a large amount of syn-tectonic deposition covering both the wedge and the fore-deep the thrust sheets are very long.

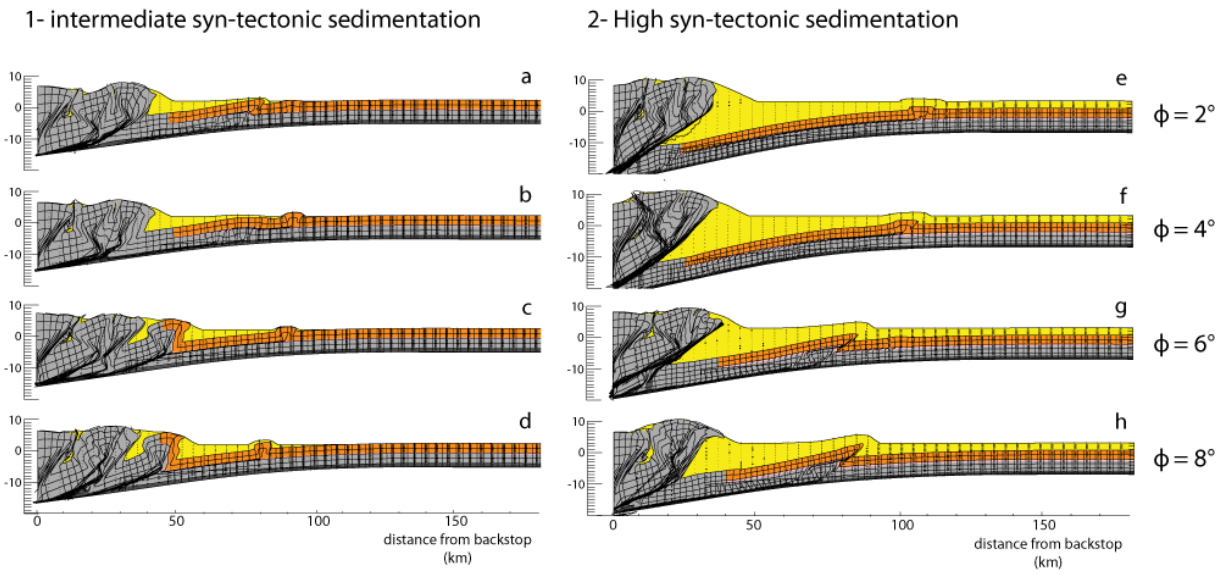

Supplementary Figure DR2: *Tests of the influence of the strength of the internal decollement on thrust sheet length. For models a to d, model set up is the same as in model 2 (Figure 2) but with syn-tectonic sedimentation starting at 3 Ma. For models e to h, the reference elevation for the syn-tectonic sedimentation was set to 3 km, resulting in sediments covering the complete foreland basin. The strength of the décollement is represented by the internal friction angle ϕ, that is 2°, 4°, 6°, and 8° for models a and e, b and f ,c and g , d and h respectively. Models snapshots are shown at the time when the first external thrust activates.*

Strain rates and velocity field

Supplementary Figure S3 documents the strain-rate evolution for the same models and at the same timesteps as shown in Figure 2. The green zones (at 7 m.y. in models 1 and 3 for example) show the diffuse pattern of strain partitioning that is subsequently followed by localization on large faults. In the three models, most of the material advection from the right side of the model is accommodated by the fontal thrust and by underthrusting below the décollement level. In Model 1 (without syn-tectonic sedimentation), at 5 my, displacement is localized at the front but in the internal parts as well, with active backthrusting at around 50 km. Then this internal displacement progressively decreases to almost zero at

12 m.y. The velocity field in the fold-and-thrust belt shows that each thrust is active, but always less than the frontal thrust. Model 2 and 3 are very similar in terms of velocity field patterns. The backthrusting that occurs at 5 m.y. is very efficient at that time while the internal part experiences little displacement. Between 7 and 9 m.y. the frontal thrust records most of the displacement, and the internal part (especially around 50 km from the backstop) show moderate and upward-directed velocities. Finally, at 12 m.y., only the fold-and-thrust belt records displacement, and the internal part become much less active. It is also worth noting that the velocity field shows the progression of under-thusting below the internal decollement level towards the left side of the model. Strain localization allows identifying the most active faults. In the three models, the strain is accumulated on 1) the frontal thrust, 2) the décollement level, and 3) the largest shear zones in the internal parts, with the décollement level concentrating most strain.

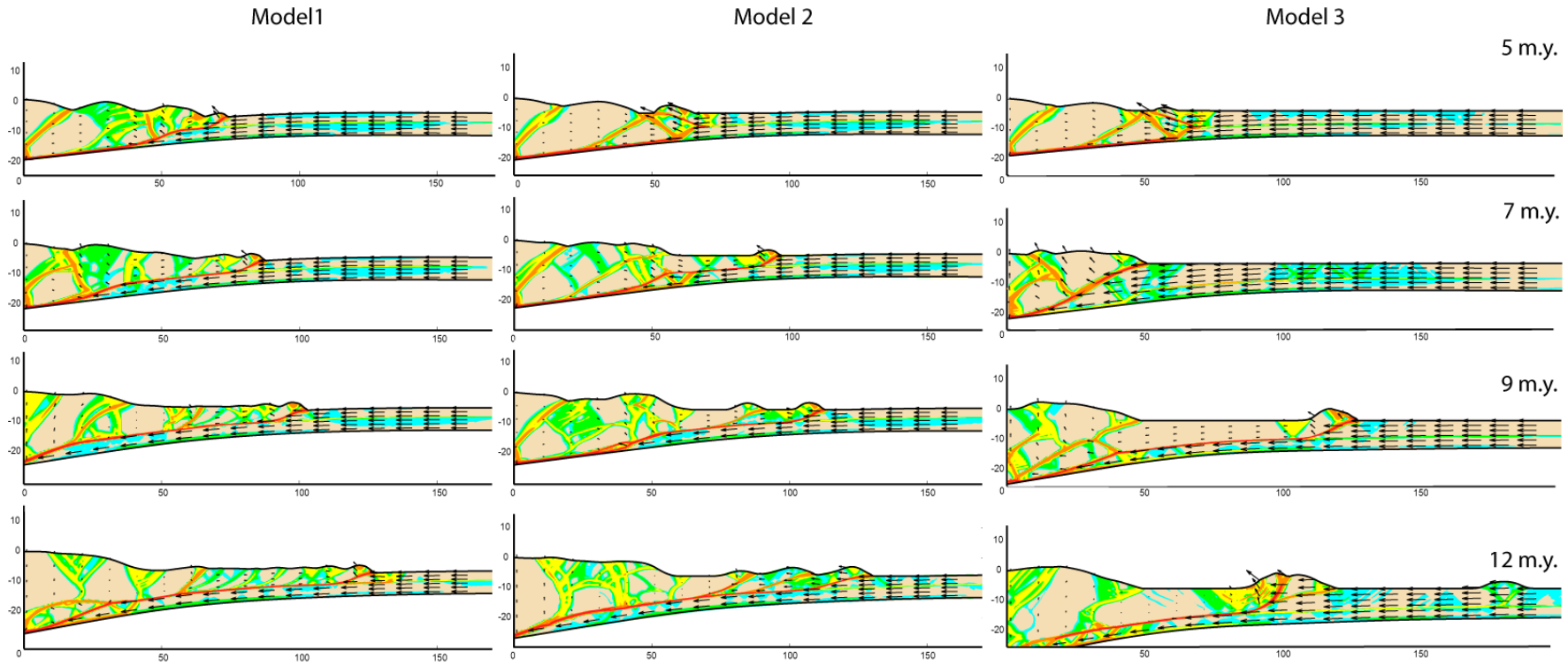

Supplementary Figure DR3*: Evolution of second invariant of deviatoric strain rate and velocity field for models/snapshots shown in Figure 2 (main paper).*

Data and references for Natural Systems

Supplementary Table 2*: Sediment thicknesses, thrust-sheet lengths, and equivalent elastic thicknesses for natural fold-and-thrust belts. Measurements of thrust sheet length and their associated syn-tectonic sedimentation thickness was taken in three places of the fold-and thrust belt at least .The sediment thickness was measured at the place where the vertical thickness is maximum, i.e in the center of a piggy-back basin for example. The thrust sheet length was defined by the length from the place where the thrust is differentiating to its surface emergence.*

Range	Average thrust length (km)	Maximum thickness of syn-tectonic sediments (km)	Reference for cross-sections	Elastic thickness (km)	Reference for Te
Canadian Rockies (Can)	5.5 ± 3.1	1.5 ± 0.7	*Ollerenshaw, 1978*	20 to 40	*Flück et al., 2003*
Sub-andean belt (An2, S Bolivia)	6.3 ± 2.2	1.5 ± 0.3	*Horton, 1998*	30 to 40	*DeCelles and Horton, 2003a*
Apennines (Ap)	8.6 ± 4.1	1.8 ± 0.6	*Butler et al., 2004*	8 to 15	*Royden and Karner, 1984*
Carpathians (Car)	12.9 ± 1.4	1.5 ± 0.6	*Hippolyte et al., 1999*	3 to 16	*Zoetemeijer et al., 1999*
Pyrenees (Pyr)	13.8 ± 4.6	2.5 ± 0.3	*Muñoz, 1992*	20 to 30	*Zoetemeijer et al., 1990*
Swiss molassic basin (Alp)	14 ± 2	1.5 ± 0.3	*Beck et al., 1998*	5 to 15	*Sinclair et al., 1991*
Sub-andean belt (An1, NW Bolivia)	15.6 ± 4.3	3.1 ± 0.8	*Baby et al., 1995*	30 to 40	*DeCelles and Horton, 2003b*
Brooks ranges (Br)	20 ± 5	1 ± 0.2	*Cole et al., 1997*	65 to 75	*Nunn et al., 1987*

References

Baby, P., Limachi, R., Moretti, I., Mendez, E., Oller, J., Guiller, B., and Specht, M., 1995, Petroleum system of the northern and central Bolivian sub-Andean zone, *in* A.J.Tankard, Suarez, R., and Welsink, H.J., eds., Petroleum Basins of South America, Volume American Association of Petroleum Geologists Memoir, 62, p. 445-458.

Beck, C., Deville, E., Blanc, E., Philippe, Y., and Tardy, M., 1998, Termination of the Savoy Molasse Basin (northwestern siliciclastic accumulation (Upper Marine Molasse) in the southern Alps/southern Jura), *in* Mascle, A., Puigdefàbregas, C., Luterbacher, H.P., and Fernàndez, M., eds., Cenozoic Foreland Basins of Western Europe, Volume Geological Society, London, Special Publication, 134, p. 263-278.

Butler, R.W.H., Mazzoli, S., Corrado, S., De Donatis, M., Di Bucci, D., Gambini, R., Naso, G., Nicolai, C., Scrocca, D., Shiner, P., and Zucconi, V., 2004, Applying thick-skinned tectonic models to the Apennine thrust belt of Italy—Limitations and implications, *in* McClay, K.R., ed., Thrust tectonics and hydrocarbon systems, Volume 82, p. 647– 667.

Cole, F., Bird, K.J., Toro, J., Roure, F., O'Sullivan, P.B., Pawlewicz, M., and Howell, D.G., 1997, An integrated model for the tectonic development of the frontal Brooks Range and Colville Basin 250 km west of the Trans-Alaska Crustal Transect: Journal of Geophysical Research, v. 102, p. 20685-20708.

DeCelles, P., and Horton, B.K., 2003a, Early to middle Tertiary foreland basin development and the history of Andean crustal shortening in Bolivia: GSA Bulletin, v. 115, p. 58-77.

DeCelles, P., and Horton, B.K, 2003b, Early to middle Tertiary foreland basin development and the history of Andean crustal shortening in Bolivia: Geological Society of America Bulletin, v. 115, p. 58-77.

Flück, P., Hyndman, R.D., and Lowe, C., 2003, Effective elastic thickness T e of the lithosphere in western Canada: Journal of Geophysical Research, v. 108, p. 2430.

Hippolyte, J.C., Badescu, D., and Constantin, P., 1999, Evolution of the transport direction of the Carpathian belt during its collision with the east European Platform: Tectonics, v. 18, p. 1120-1138.

Horton, B.K., 1998, Sediment accumulation on top of the Andean orogenic wedge: Oligocene to late Miocene basins of the Eastern Cordillera, southern Bolivia: Geological Society of America Bulletin, v. 110, p. 1174-1192.

Huismans, R.S., and Beaumont, C., 2007, Roles of lithospheric strain softening and heterogeneity in determining the geometry of rifts and continental margins, *in* Karner, G.D., Manatschal, G., & Pinhiero, L.M. , ed., Imaging, Mapping and Modelling Continental Lithosphere Extension and Breakup, Geological Society, London, Special Publications, p. 107-134.

Muñoz, J.A., 1992, Evolution of a continental collision belt: ECORS Pyrenees crustal balanced cross section, *in* McClay, K.R., ed., Thrust Tectonics: London, Chapman & Hall, p. 235-246.

Nunn, J.A., Czerniak, M., and Pilger, R.H.J., 1987, Constraints on the structure of Brooks Range and Colville Basin, Northern Alaska, from flexure and gravity analysis.: Tectonics, v. 6, p. 603-617.

Ollerenshaw, N.C., 1978, Geology, Calgary, Alberta–British Columbia, Geological Survey of Canada Map 1457A.

Royden, L., and Karner, G.D., 1984, Flexure of Lithosphere Beneath Apennine and Carpathian Foredeep Basins: Evidence for an Insufficient Topographic Load: AAPG Bulletin, v. 68.

Sinclair, H.D., Coakley, B.J., Allen, P.A., and Watts, A.B., 1991, Simulation of Foreland Basin Stratigraphy using a diffusion model of mountain belt uplift and erosion: An example from the central Alps, Switzerland: Tectonics, v. 10, p. 599-620.

Zoetemeijer, R., Desegaulx, P., Cloetingh, S., Roure, F., and Moretti, I., 1990, Lithospheric Dynamics and Tectonic-startigraphic Evolution of the Ebro basin: Journal of Geophysical Research, v. 95, p. 2701-2711.

Zoetemeijer, R., Tomek, C., and Cloetingh, S., 1999, Flexural expression of European continental lithosphere under the western outer Carpathians: Tectonics, v. 18, p. 843-861.